Science of the Total Environment 948 (2024) 174725

Contents lists available at ScienceDirect

Science of the Total Environment

journal homepage: www.elsevier.com/locate/scitotenv

Kinetics and toxicity of nanoplastics in *ex vivo* exposed human whole blood as a model to understand their impact on human health

J. Arribas Arranz [a], A. Villacorta [a,b], L. Rubio [a], A. García-Rodríguez [a], G. Sánchez [c], M. Llorca [d], M. Farre [d], J.F. Ferrer [e], R. Marcos [a,*], A. Hernández [a,*]

[a] Group of Mutagenesis, Department of Genetics and Microbiology, Faculty of Biosciences, Universitat Autònoma de Barcelona, Cerdanyola del Vallès, Barcelona, Spain
[b] Facultad de Recursos Naturales Renovables, Universidad Arturo Prat, Iquique, Chile
[c] Institute of Agrochemistry and Food Technology, IATA-CSIC, Av. Agustín Escardino 7, Paterna, Valencia 46980, Spain
[d] Department of Environmental Chemistry, Institute of Environmental Assessment and Water Research (IDÆA-CSIC), 08034 Barcelona, Spain
[e] AIMPLAS, Plastics Technology Center, Valencia Parc Tecnologic, 46980 Paterna, Spain

HIGHLIGHTS

- The effects of nanoplastics (NPLs) on human blood were evaluated.
- Five different NPLs and blood from eight healthy donors were used.
- Internalization, ROS, cytokine release, hemolysis, and platelet functionality were determined.
- Differential effects, except for platelet functionality, were observed according to NPL and target.
- This is the first study comprehensively evaluating bloodstream kinetics and toxicity of NPLs.

GRAPHICAL ABSTRACT

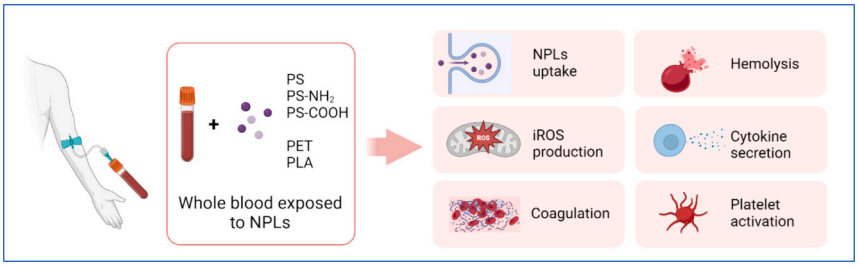

ARTICLE INFO

Editor: Lidia Minguez Alarcon

Keywords:
Nanoplastics
Uptake
Oxidative stress
Hemolysis
Platelets functionality

ABSTRACT

The ubiquitous presence of nanoplastics (NPLs) in the environment is considered of great health concern. Due to their size, NPLs can cross both the intestinal and pulmonary barriers and, consequently, their presence in the blood compartment is expected. Understanding the interactions between NPLs and human blood components is required. In this study, to simulate more adequate real exposure conditions, the whole blood of healthy donors was exposed to five different NPLs: three polystyrene NPLs of approximately 50 nm (aminated PS-NH_2, carboxylated PS-COOH, and pristine PS- forms), together with two *true-to-life* NPLs from polyethylene terephthalate (PET) and polylactic acid (PLA) of about 150 nm. Internalization was determined in white blood cells (WBCs) by confocal microscopy, once the different main cell subtypes (monocytes, polymorphonucleated cells, and lymphocytes) were sorted by flow cytometry. Intracellular reactive oxygen species (iROS) induction was determined in WBCs and cytokine release in plasma. In addition, hemolysis, coagulation, and platelet activation were also determined. Results showed a differential uptake between WBC subtypes, with monocytes showing a higher internalization. Regarding iROS, lymphocytes were those with higher levels, which was observed for different NPLs. Changes in cytokine release were also detected, with higher effects observed after PLA- and PS-NH_2-NPL exposure. Hemolysis induction was observed after PS- and PS-COOH-NPL exposure, but no effects on platelet functionality were observed after any of the treatments. To our knowledge, this is the first study

* Corresponding authors at: Group of Mutagenesis, Department of Genetics and Microbiology, Faculty of Biosciences, Universitat Autònoma de Barcelona, Campus of Bellaterra, 08193 Cerdanyola del Vallès, Barcelona, Spain.
E-mail addresses: ricard.marcos@uab.cat (R. Marcos), alba.hernandez@uab.cat (A. Hernández).

https://doi.org/10.1016/j.scitotenv.2024.174725
Received 29 May 2024; Received in revised form 9 July 2024; Accepted 10 July 2024
Available online 14 July 2024

comprehensively evaluating the bloodstream kinetics and toxicity of NPL from different polymeric types on human whole blood, considering the role played by the cell subtype and the NPLs physicochemical characteristics in the effects observed after the exposures.

1. Introduction

Micro and nanoplastics (MNPLs) are tiny plastic particles ubiquitous in the environment due to the widespread use of plastic materials and their improper disposal. Environmental factors such as UV radiation, mechanical action, and biological processes contribute to breaking down plastic materials into smaller particles to MNPLs. They may also be intentionally produced for various purposes or as byproducts of industrial processes. Because of their ubiquitous presence, MNPLs represent significant challenges in terms of environmental pollution and human health risk (Rubio et al., 2020; Landrigan et al., 2023).

While microplastics (MPLs) have been the subject of intense research, the study of nanoplastics (NPLs) is a relatively nascent field demanding attention. NPLs, ranging from 1 to 1000 nm, offer unique physicochemical properties that permit translocation through biological barriers, reaching the bloodstream and permitting their distribution to organs and tissues (Ramsperger et al., 2023). Indeed, NPLs of approximately 700 nm have been detected in human whole blood samples representative of the general population, PET- and PS-MNPLs are the most widely encountered (Leslie et al., 2022). Accordingly, the potential interaction between NPLs and blood components requires further research. Nanoparticles can translocate the endothelial barrier using an active process through endothelial cells (trans-endothelial) or the gaps between endothelial cells (inter-endothelial gaps). The size of these gaps was up to 2000 nm, which is the size allowing translocation (Sindhwani et al., 2020).

Blood consists of plasma and different cell types such as leukocytes (WBCs), erythrocytes, and platelets, suspended in the plasma together with other molecules, such as various complement proteins and immunoglobulins. NPLs, by entering the bloodstream, can directly or indirectly interact with these cells or blood components, potentially influencing their structure and function. White blood cells (WBC) are classified as monocytes, polymorphonucleated cells (PMNs), and lymphocytes, playing an essential role in inflammation, host defense systems, and immunity. In blood, monocytes and PMNs, travel through the body acting as scavengers to recognize, attack, and engulf foreign particles, and remove pathogens, and old or dead cells. Also, several types of WBC can synthesize cytokines that are essential for cell-to-cell signaling, and for the synchronization of the various parts of the immune system (Altan-Bonnet and Mukherjee, 2019). Some studies have reported genotoxic damage and oxidative stress in lymphocytes and monocytes by NPL exposure (Ballesteros et al., 2020; Sarma et al., 2022). Other studies have linked NPLs exposure to disruption of the immune system in invertebrates (Brandts et al., 2018; Auguste et al., 2020; Zhou et al., 2023), fishes (Greven et al., 2016; Brandts et al., 2018), and mice, showing a significant immune activation after inhaling polystyrene NPLs that lead to pulmonary toxicity (Wu et al., 2023a). In line with this, in previous studies on the immunotoxicity of polystyrene NPLs, alterations in the whole blood secretome were reported (Ballesteros et al., 2020), and similar effects were observed after nanoparticle exposures, such as graphene-based nanomaterials (Ballesteros et al., 2021). Erythrocytes are the main component of blood and for some times have been considered inert and only responsible for the transportation of gases and nutrients throughout the human body. Nevertheless, clinical and epidemiological studies showed that they play an important role in cardiovascular homeostasis by promoting the coagulation cascade and thrombus formation in venous thrombosis (Byrnes and Wolberg, 2017). Because of the increasing clinical interest in MNPLs as potential drug carriers, some studies have tested some NPLs in human blood cells showing that they can attach to the surface of erythrocytes, altering their aggregation and adhesion (Tian et al., 2021). Platelets are multifunctional enucleated cells involved in many processes including hemostasis and thrombosis, clot retraction, vessel constriction and repair, inflammation including promotion of atherosclerosis, host defense, and even tumor growth and metastasis (van der Meijden and Heemskerk, 2019). Although different engineered nanoparticles have been shown to affect platelet function (Matus et al., 2018), little is known about the effects of NPLs on platelet physiology and functions. White blood cells (WBC) are classified as monocytes, polymorphonucleated cells (PMNs), and lymphocytes, playing an essential role in inflammation, host defense systems, and immunity. In blood, monocytes and PMNs, travel through the body acting as scavengers to recognize, attack, and engulf foreign particles, and remove pathogens, and old or dead cells. Also, several types of WBC can synthesize cytokines that are essential for cell-to-cell signaling and for the synchronization of the various parts of the immune system (Altan-Bonnet and Mukherjee, 2019). Some studies have reported genotoxic damage and oxidative stress in lymphocytes and monocytes by NPL exposure (Ballesteros et al., 2020; Sarma et al., 2022). Other studies have linked NPLs exposure to disruption of the immune system in invertebrates (Brandts et al., 2018; Auguste et al., 2020; Zhou et al., 2023), fishes (Greven et al., 2016; Brandts et al., 2018), and mice, showing a significant immune activation after inhaling polystyrene NPLs that lead to pulmonary toxicity (Wu et al., 2023a). In line with this, in previous studies on the immunotoxicity of polystyrene NPLs, alterations in the whole blood secretome were reported (Ballesteros et al., 2020), and similar effects were observed after nanoparticle exposures, such as graphene-based nanomaterials (Ballesteros et al., 2021).

While some knowledge about the hemocompatibility and inflammatory effects of specific NPL exists, this has been obtained mainly from *in vitro* studies, which are far away from the complexity of whole human blood. To fill in this gap, our study aims to characterize the effects of NPLs, from different polymeric types, in human whole blood. We have used an *ex vivo* model in which whole human peripheral blood from healthy donors was exposed to different NPLs. To explore the influence of the NPL physicochemical characteristics on the analyzed effects, polystyrene nanoplastics (PS-NPLs) of around 50 nm with several surface properties were chosen: pristine, carboxyl (-COOH) surface-modification, and amino ($-NH_2$) surface-modification, changes that NPLs can acquire during their weathering processes in the environment. To determine the influence of the polymer type, in addition to polystyrene (PS-NPLs), used as the standard model of NPLs, *true-to-life* materials obtained from the degradation of plastic goods were also employed: polyethylene terephthalate (PET-NPLs, 176 nm average), and the most popular bio-based polymer polylactic acid (PLA-NPLs, 130 nm average), which provided us with a more realistic insight into what may be happening in real exposure scenarios. Firstly, we quantified the different internalization rates for each major type of WBC separately, after exposure. As cell-based endpoints, we determined the induction of intracellular reactive oxygen species (iROS) for each WBC type separately, as well as platelet activation due to NPLs exposure. In addition, we assayed NPLs' hemotoxicity measuring the hemolysis and changes in clinical coagulation parameters. Finally, to study potential secretome alterations, the expression levels of a wide panel of representative cytokines were evaluated.

Overall, our *ex vivo* model proved to be useful for determining the kinetic and effects of NPLs in a realistic context. The results could help to better understand the role of NPL internalization levels in their potential toxicity, depending on the tested cell type. They are also useful for determining which cell types and biomarkers would be appropriate to

use in human biomonitoring studies with NPL-exposed individuals, once tools for developing such studies are available and optimized, and in more in-depth and specific immune-toxicological studies.

2. Materials and methods

2.1. The selected NPLs

Different types of nanoplastics were used in this study. Commercially available pristine polystyrene nanoplastics (PS-NPLs) were purchased from various sources. At the same time, true-to-life nano polyethylene terephthalate nanoplastics (PET-NPLs) were obtained from plastic water bottle degradation (Villacorta et al., 2022), and nano polylactic acid (PLA-NPLs) from pellet degradation (Alaraby et al., 2024), according to the quoted references.

In brief, for PET-NPLs obtention, PET powder was acquired by sanding water bottle pieces with a diamond rotary burr, sieved, and dispersed by stirring in pre-heated trifluoroacetic acid. After centrifugation, the supernatant was removed, and the pellet was resuspended in sodium dodecyl sulfate and sonicated. The emulsion was allowed to settle, and the supernatant was washed with Milli-Q water and pure ethanol (to discard SDS) and left to dry. The obtained PET-NPL powder was resuspended in Milli-Q water, sonicated, aliquoted in cryotubes, and immediately frozen in liquid nitrogen. True-to-life PLA-NPLs were obtained by preparing a pre-mini emulsion in which the aqueous phase consisting of dissolved Pluronic and polyvinyl alcohol (as co-stabilizer) in 120 mL of water (0.25 % wt and 2 % wt, respectively) was added to the organic phase composed by 1 g of PLA dissolved in 30 g dichloromethane, and stirring magnetically for 60 min. Furthermore, ultrasonication under ice cooling was applied for 120 s at 80 % amplitude, and the obtained mini-emulsion was transferred to a round bottom flask to evaporate the organic solvent under pressure.

Six types of PS-NPLs were used: pristine nanopolystyrene (PS-NPLs, Spherotech, ref. PP-008-10, with particles ranging from 50 to 100 nm), fluorescent pristine nanopolystyrene (fPS-NPLs, Spherotech, ref. FP-00552-2, with particles ranging from 40 to 90 nm), carboxylated-surface nanopolystyrene (PS-COOH-NPLs, Polysciences, ref. 15913-10 with mean sized particles of 50 nm), fluorescent carboxylated-surface nanopolystyrene (fPS-COOH-NPLs, Polysciences, ref. 16661-10 with particles mean sized particles of 50 nm), aminated-surface nanopolystyrene (PS-NH_2-NPLs, Nanocs, ref. PS50-AM-1 with particles mean sized particles of 50 nm), and fluorescent aminated-surface nanopolystyrene (fPS-NH_2-NPLs, Nanocs, ref. PS50-AMFC-1 with particles mean sized particles of 50 nm). In addition, two types of *true-to-life* PET-NPLs with a mean size of 176 nm were used: non-fluorescent (PET-NPLs) and fluorescent PET (fPET-NPLs) labeled with the textile dye iDye Poly Pink according to the procedure reported by Villacorta et al. (2024). Furthermore, *true-to-life* PLA-NPLs and their fluorescent counterpart (fPLA-NPLs) with a mean size of 130 nm (Alaraby et al., 2024) were also used. Fluorescent particle staining stabilities were tested 8 months after the labeling procedure without significant fluorescence loss, also, eluent staining properties were tested on different *in vitro* cell models showing no signal (THP-1 monocytes, Raji lymphoblast-like cells, A549 lung epithelial cells, MH-S macrophages, and HUH-7 hepatic epithelial cells) (Villacorta et al., 2024).

2.2. NPLs characterization

2.2.1. Scanning electron microscopy

To confirm the characteristics (including the predicted size) of the used NPLs, further characterizations were carried out. The dry state size was assessed by scanning electron microscopy (SEM). To proceed, a single 10 μL drop at a concentration of 100 μg/mL was placed on separated coverslips and left to dry overnight inside a lid-protected Petri dish. NPLs were then inspected by SEM (Zeiss Merlin, Zeiss, Oberkochen, Germany). The acquired images were analyzed for particle size distribution by measuring the Martin diameter using the ImageJ software 1.8.0_172. At least 200 random particles were counted and analyzed for commercial NPLs (PS-, PS-COOH-, and PS-NH_2-) while no <1500 random single particles were subjected to study in the case of in-house made polymers (PLA- and PET-NPLs). Data was then processed, and charts were prepared using the GraphPad Prism 8.0 software (GraphPad, San Diego, CA, USA).

2.2.2. Dynamic Light Scattering (DLS)

The hydrodynamic behavior as the indicative size of colloid structures in Milli-Q water suspensions of the different NPLs was determined using a Zetasizer® Ultra device from Malvern Panalytical (Cambridge, UK). Shortly, working solutions were independently prepared for each particle suspension at a final concentration of 100 μg/mL. One milliliter aliquot of each suspension was transferred to a DTS0012 cuvette and data was acquired with a collection angle of 174.8°. For the *Z*-potential determination, a slightly small volume of the same aliquot was transferred to a DTS1070 cuvette and analyzed using the same equipment. For all determinations, three independent measurements were carried out. Data was analyzed, and charts were prepared, using GraphPad prism 8.0 (GraphPad, San Diego, CA).

2.3. Blood sample collection and ex vivo NPLs exposure

Peripheral blood samples from medium-aged healthy donors (a total of 5 women and 3 men between 25 and 45 years old) were collected and stabilized with heparin (1 %), except for the coagulation assays for which citrate (1 %) was used as an anticoagulant. Informed written consent was obtained from all participants, and the Ethics Committee of the Autonomous University of Barcelona approved the protocol according to the Declaration of Helsinki.

For each experiment, blood samples were divided into six 3 mL aliquots within the first hour after collection and exposed, except for the negative control, to the different NPLs (PS, PS-NH_2, PS-COOH, PET, and PLA) at a final concentration of 100 μg/mL for 24 h at 37 °C and 80 rpm constant agitation (as previously described in Ballesteros et al., 2021). This concentration was chosen to ensure significant internalization rates across all treatments and cell subtypes while maintaining a sub-toxic concentration as described in previous studies (Martín-Pérez et al., 2024). The non-fluorescent versions of the different NPLs were used in all approaches except for internalization studies and for sorting cell populations with internalized NPLs and their subsequent visualization using confocal microscopy, as well as for their analysis of iROS content, where fluorescent versions of the NPLs were used for cell sorting.

2.4. Whole blood fractionation

2.4.1. Plasma isolation for cytokine characterization, platelet activation, and coagulation assays

Blood-exposed samples were centrifuged at 1500 *g* for 10 min to separate the plasma from the cellular pellet. Plasma samples were collected and immediately processed for the coagulation assays or stored at −80 °C for later analysis (Ballesteros et al., 2021).

2.4.2. WBCs isolation for internalization and ROS generation assays

To isolate the white blood cells (WBCs), erythrocytes were lysed with erythrocyte lysis buffer (NH_4Cl 0.15 M; HCO_3 0.01 M; EDTA 0.1 mM; pH 7.1–7.4) for 10 min in agitation. After that, cells were centrifuged at 400 *g* for 5 min, the supernatant was discarded, and the cells were resuspended, washed with PBS, and centrifuged at 400 *g* for 5 min. This procedure was repeated once more with centrifugations at 250 g for 10 min, to obtain WBC pellets (Ballesteros et al., 2021).

2.4.3. Erythrocyte suspension preparation for hemolysis assays

To measure the potential hemolytic effect of the NPLs, erythrocyte suspensions were prepared by centrifuging the blood at 1500 g for 10

min. After discarding the plasma, the hematocrit level was filled to the original volume with PBS and washed three times with PBS. Dilutions 1:50 of the hematocrit were used for the hemolysis assay (Urbán et al., 2019).

2.5. SEM visualization of NPLs in whole blood

NPL-cell interactions were visualized by SEM (Zeiss Merlin, Zeiss, Oberkochen, Germany). Briefly, exposed whole blood samples were centrifuged at 1500 *g* for 10 min and 100 μL of sample was recovered from the interface between plasma and cells, and placed in 12 mm Ø cover slip poly-L-lysine coated for 5 min at 25 °C. Then, 200 μL 0.2 M $CaCl_2$ was added on the top of the blood cells to activate the platelets and left for 10 min. Samples were fixed by adding 4 % paraformaldehyde, and 0.4 % glutaraldehyde in 0.2 M sodium cacodylate buffer, pH 7.2, on the top of the blood cells and left at least for 10 min. Then samples were dehydrated and coated with 6 nm of platinum/palladium. Dried coverslips were mounted on stubs containing carbon adhesives (Agar Scientific, Ltd., UK). Finally, representative images were taken from a random field of view. NPLs were artificially colored in blue with Photoshop software to present better the diverse localizations of the different blood cell subtypes.

2.6. Quantification of NPLs uptake in WBCs by flow cytometry

Control and exposed WBCs were resuspended in PBS and incubated with BD *Via*-Probe™ (Biosciences ref. 555816) to discriminate dead/live cells. For gating cells, each population of WBCs (lymphocytes, monocytes, and PMNs) was carefully chosen by FSC-H and SSC-H and separated according to their complexity and size. The intracellular fluorescence was measured using a CytoFlex flow cytometer (Beckman Coulter) and 20,000 cells were evaluated using the CytoFlex software. At least three independent experiments were carried out for each NPLs using whole blood from seven different donors (Ballesteros et al., 2021).

2.7. Visualization of NPLs uptake in WBCs by confocal imaging

A BD FACSJazz™ cell sorter (BD Biosciences) was used to select and separate WBCs previously exposed for 24 h to 100 μg/mL of the fluorescent NPLs (fPS, fPS-NH_2, fPS-COOH, fPET, and fPLA). The drop frequency was 39.05 kHz, the sheath pressure used was 27 psi, and the piezo amplitude of 1.63. The acquisition speed was up to 4000 events per second. The sorting mode was 1 drop pure, and the rate varied between 1000 and 1500 cells/s, depending on the sample. Before the sorting, incubation with BD *Via*-Probe™ (Biosciences ref. 555816) was carried out to avoid sorting dead cells. For gating cells, each population of WBCs (lymphocytes, monocytes, and PMNs) was carefully chosen by FSC-H and SSC-H. Then, single cells with intracellular fluorescence were selected and deposited in 5 % BSA PBS for confocal imaging.

Confocal microscopy was used to confirm and visualize the cellular uptake of fluorescent NPLs by the different sub-populations of WBCs obtained by sorting. To proceed, cells were incubated for 15 min with 1:500 Cellmask™ Deep Red plasma (ThermoFisher Scientific) and 1:500 Hoechst 33342 (ThermoFisher Scientific), to stain the cell membranes and the nuclei, respectively. Confocal images were acquired sequentially with a Leica TCS SP5 confocal microscope (Leica). Three different lasers were used to visualize the nucleus (405 nm), the plasma membrane (635 nm), and the fluorescent NPLs (585 nm). ImageJ software was used to analyze and process the obtained images.

2.8. Intracellular reactive oxygen species (iROS)

The induction of iROS such as cytosolic superoxide by NPL exposure was quantified by using the dihydroethidium assay (DHE), as recently published (Banaei et al., 2023). After WBCs isolation, cells were resuspended on 10 μM DHE diluted on PBS and incubated for 30 min at 37 °C. Cells with internalized NPLs were sorted and analyzed by flow cytometry (Beckman Coulter CytoFLEX). A total number of 20,000 events (single cells) were scored and evaluated using the CytExpert software. A minimum of three independent experiments with three different donors were carried out.

2.9. Plasma cytokines detection

The Human XL Cytokine Array Kit (R&D Systems Bio-techne, Proteome Profiler™) was used to determine changes in cytokine expression induced by NPL exposure, following the manufacturer instructions. Briefly, after blocking, the array was incubated with 350 μL of plasma overnight at 4 °C on a rocking platform shaker. The array was washed 3 times with washing buffer to remove unbound proteins and incubated with a cocktail of biotinylated detection antibodies for 1 h at room temperature. Streptavidin-HRP and chemiluminescent detection reagents were then applied, and a signal was generated at each antibody spot on the array membrane with an intensity corresponding to the amount of bound protein. The membranes were visualized using an enhanced chemiluminescence system (ECL, Cell Signaling Technologies), and the relative quantification of cytokine expression was determined using the ImageJ Protein Array tool. For cytokine array analysis, technical duplicates were considered for each plasma sample. Relative cytokine secretion for each NPL exposure was calculated as fold change relative to the unexposed whole blood control. Two independent experiments with two different donors were performed.

2.10. Hemolysis activity

The hemolysis activity induced by different NPLs was assayed using a protocol adapted from Evans et al. (2013). Briefly, 1 mL of 1:50 dilution in PBS of washed and packed erythrocytes was incubated for 24 h at 37 °C in mild agitation (80 rpm) with the different NPLs at 100 μg/mL. 10 % Triton X-100 and PBS, incubated with diluted erythrocyte suspensions, served as positive and negative controls, respectively. The mixtures were then centrifuged at 900 *g* for 10 min, and 100 μL of the supernatants were transferred to a flat-bottomed 96-well plate to measure the absorbance at 450 nm with a plate reader (Sunrise, Tecan) using the XFLUOR4 software.

The following formula was used to calculate the hemolysis percentage:

$$\%\text{hemolysis} = 100 \cdot \frac{(\text{sample absorbance} - \text{negative control absorbance})}{(\text{positive control absorbance} - \text{negative control absorbance})}$$

Mean ± SEM values were calculated from a minimum of 3 independent experiments with blood from 3 different healthy donors.

2.11. Coagulation assays

The clinical laboratory Laboratorios Echevarne (Registered with Health Dept) externally performed the blood coagulation tests.

Activated partial thromboplastin time (aPTT), prothrombin time (PT), thrombin time (TT), and fibrin (FIB), referred to as the four major indexes in blood coagulation function assessment, were analyzed. The relative levels of the parameters in the exposed blood *versus* the control sample were obtained from two different donors in two independent experiments and represented as mean ± SEM.

2.12. Platelet activation

To study the platelet activation after NPLs exposure, plasma thromboxane B_2 was quantified with the Parameter™ Thromboxane B_2 Immunoassay (R&D Systems Bio-techne) following the manufacturer's protocol, and as reflected in the literature (Helgadóttir et al., 2019). Mean ± SEM values were calculated from a minimum of 3 independent experiments with blood from 3 different healthy donors.

2.13. Statistical analysis

Data analysis was performed using GraphPad Prism 9 software (GraphPad Software Inc., CA, USA). To test the normal distribution of our data, the Shapiro-Wilk test was used, followed by the one-way ANOVA with Tukey's multiple comparisons test as parametric tests, or the Kruskal-Wallis tests as non-parametric. Statistical significance was depicted as $*p \leq 0.05$, $**p \leq 0.01$ and $***p \leq 0.001$.

3. Results and discussion

3.1. NPLs characterization

Due to their unique physicochemical properties, NPLs particles can translocate through biological barriers, reach the bloodstream, and be distributed to organs and tissues. Two relevant parameters of NPLs, such as size and aggregation potential, are crucial to modulating their interaction with biological barriers. Thus, size in a dry state was assessed by SEM, and the behavior in suspension was assessed by DLS. All obtained data is summarized in Table 1, and graphic representations are available on supplementary material for DLS and SEM size distribution (Fig. S1), as well as for the correlation curves (Fig. S2). The nanoparticle size, as measured by the Martin diameter, results in a highly monodispersed size distribution for all engineered pristine PS materials. Similar behavior was observed on suspension, with the remarkable exception of PS-NH_2-NPLs which increased the light dispersion and therefore the aggregation by 3.75 folds, even though the values remain on the nanoscale range. For the in-house obtained polymers (PET- and PLA-NPLs) the polydispersity indexes remain high, accentuating the *true-to-life* nature of the samples and therefore acknowledging the representativeness of the material more likely to be found in the environment. Even though the average sizes for both NPLs are between 100 and 200 nm, the polydispersity of PET-NPLs is higher than PLA-NPLs, but even considering this difference we were only able to detect 1.2 % of the particles over 500 nm, of which only 0.53 % are agglomerates over 1000 nm. On the other hand, 99.90 % of PLA-NPL sizes are below 500 nm. Overall, the particles that tend to show an aggregation on suspension are the ones having *Z*-potential values comparatively closer to 0. However, it should be remarked that none of the reported values fall within what is considered an instability zone. Thus, the interpretation of the observed aggregations may be due to the intrinsic polydispersity nature of the *true-to-life* particles, to its shape irregularities, or even surface functionalization, as happened in PS-NH_2-NPLs, more than to the Z-values alone. The size and aggregation potential of NPL fluorescent versions were not significantly different from the non-fluorescent parental ones (Table S1). For labeled NPLs, no significant changes were noticeable except for a decrease in size for fPLA-NPLs, coherent with a smaller Z-potential value which may indicate a less aggregate state (Martín-Pérez et al., 2024). In addition, a non-neglectable shift to positive values for PS-NH_2-NPLs was observed that does not seem to affect the hydrodynamic behavior of the suspensions. Overall, the different behavior observed between commercially available PS-NPLs and the *true-to-life* PET- and PLA-NPLs point out the importance of working with representative true-to-life NPLs in toxicology studies.

3.2. NPLs visualization in whole-blood by SEM

Due to the novelty of the work and the lack of previous knowledge about the behavior of NPLs in whole blood, the first step of our study was to prove if NPLs could interact with the different blood cell subtypes in the entire blood matrix. With this aim, SEM images of samples exposed to the different NPLs were taken (Fig. 1). As seen in the pictures, all NPLs were found physically interacting with the various blood subtypes. Although the presence of MNPLs in blood has already been demonstrated (Leslie et al., 2022), the precise localization of MNPLs has never been determined, neither in the plasma nor attached to specific blood cell subtypes. From this point of view, the images indicate that MNPLs can physically interact with all blood cell subtypes at a similar rate. It must be highlighted that no *ex vivo* studies looking for the interaction between MNPLs and whole blood cells have been reported until now. These results would suggest that the presence of MNPLs in human blood could trigger their uptake by the different cell subtypes.

3.3. Uptake of NPLs in the different blood cell subtypes

To assess the potential uptake of NPLs by the different WBCs separately (monocytes, PMNs, and lymphocytes), two different complementary methods have been used: flow cytometry, to quantify the internalization capacities, and confocal microscopy, to visualize the exact NPLs localization in sorted cells exposed to NPLs. The confocal images of the gated cells, selecting only the fluorescent cells for each population classified by FSC-H and SSC-H, revealed that the five types of NPLs studied can be internalized by the three main populations of WBC. They were mostly present in the cytoplasm and surrounded by cell membranes –most probably from endocytosis– in the case of PS-, PS-COOH-, and PET-NPLs, as changes from green to yellow color suggest (Fig. 2).

Flow cytometry was used to quantify the cellular uptake of the different NPLs. The intracellular presence of labeled NPLs in the exposed cells was taken as a measure of the percentage of cells containing NPLs (Fig. 3). Cells were classified as fluorescent (NPLs uptake) and non-fluorescent (no NPLs internalization). Results indicated both cell- and NPL-dependent internalization rates.

Table 1
NPLs characterization by DLS and SEM. Hydrodynamic and dry state average sizes of the used NPLs. Data are represented as mean ± SD ($n = 3$).

		Hydrodynamic			Dry state	
Polymer	Func	Z-average	PDI	Z-pot	Z-average	PDI
PS	–	94.00 ± 0.86	0.03	−44.90 ± 0.49	75.63 ± 0.57	0.02
PS	NH_2	213.00 ± 28.30	0.42	−21.80 ± 1.11	56.58 ± 0.69	0.03
PS	COOH	60.10 ± 0.30	0.04	−43.20 ± 0.78	54.39 ± 0.71	0.04
PET	–	343.00 ± 18.90	0.51	−26.00 ± 0.84	176.24 ± 6.52	2.05
PLA	–	538.00 ± 21.50	0.59	−21.20 ± 1.51	130.06 ± 1.51	0.19

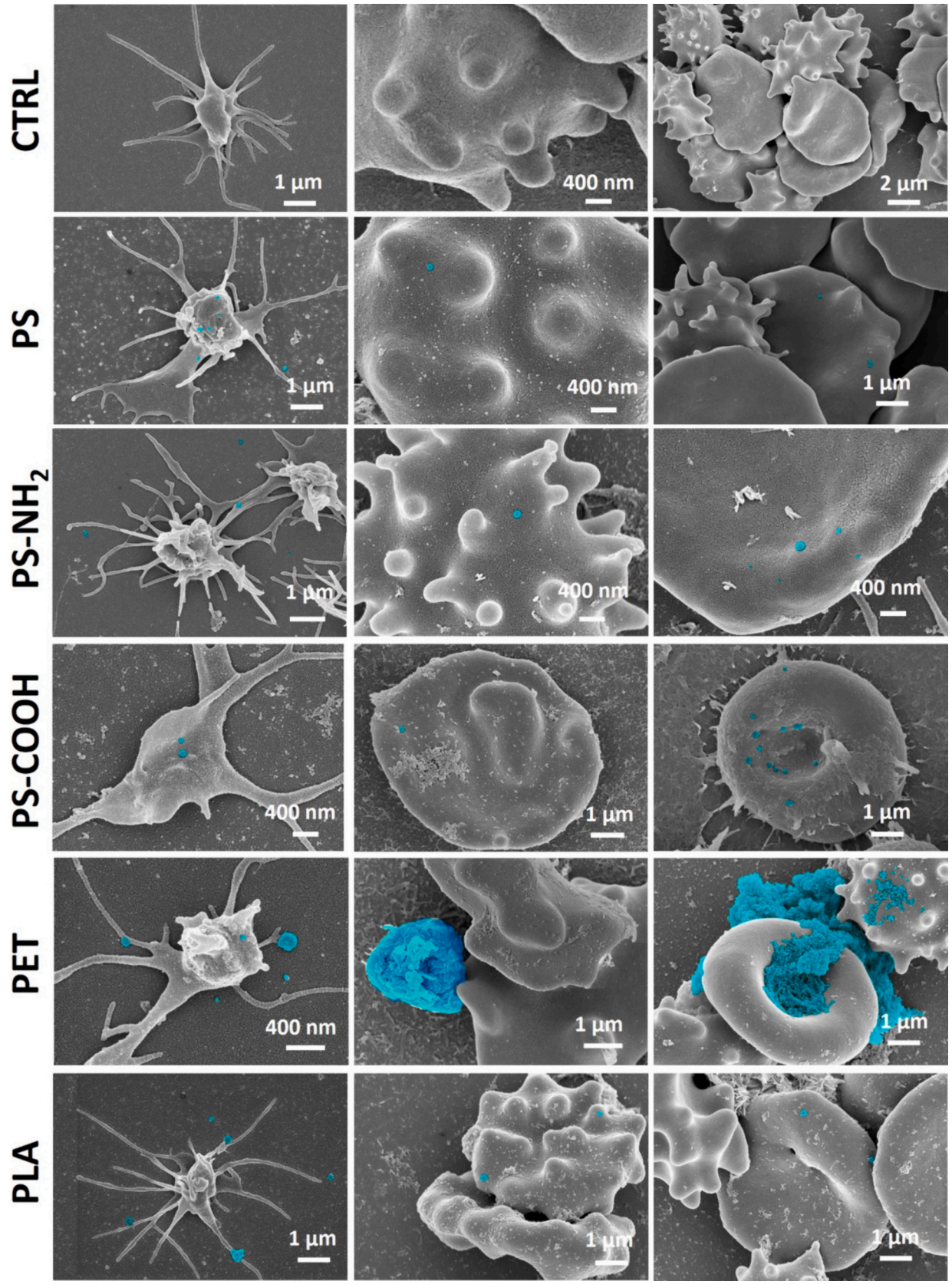

Fig. 1. Scanning electron microscope (SEM) images from NPLs-exposed and unexposed human whole blood samples. NPLs are artificially colored in blue to better present the diverse localizations of the different blood cell subtypes. The left column is platelets; the middle column has different cell subtypes; the right column is mainly erythrocytes.

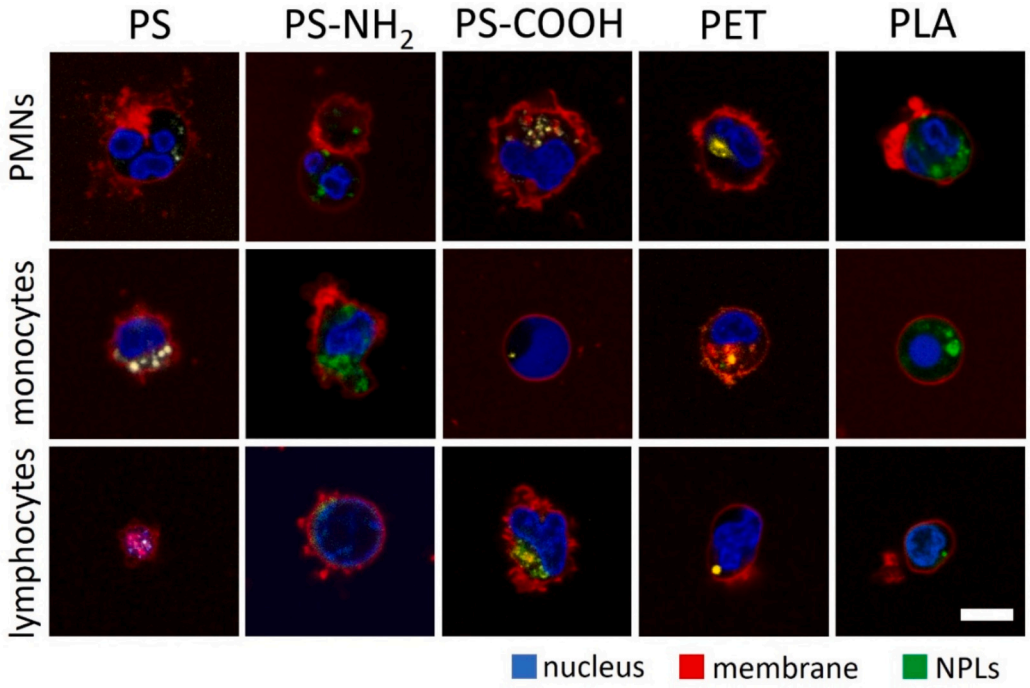

Fig. 2. Confocal imaging of the cellular internalization of the NPLs in the different sorted WBC populations (PMNs, monocytes, and lymphocytes) after exposures (100 μg/mL) lasting for 24 h. Cells were stained for the nucleus with Hoechst (blue) and the cell membrane with Cellmask™ Deep Red (red). NPLs are indicated in green or yellow (if covered with a cell membrane). Scale bar = 10 μm.

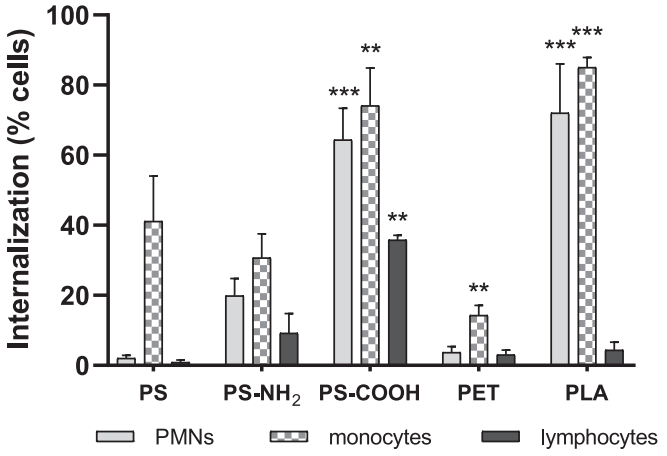

Fig. 3. NPLs internalization by the different WBC subtypes, after exposures (100 μg/mL) lasting for 24 h. The graph represents the percentage of fluorescent-positive cells over the total cell population. Graphs show the mean ± SEM. *** ($p \leq 0.001$), and ** ($p \leq 0.01$) in front of PS-NPLs exposed WBC subtypes.

Monocytes were those showing the highest internalization rate, which would agree with their role in the phagocytic system. The percentage of PMNs with internalized NPLs depended on the type of NPLs, with a similar uptake rate as monocytes in the case of PS-NH_2-, PS-COOH-, and PLA-NPLs, but lower for PS- and PET-NPLs. On the other hand, lymphocytes were the population with the lowest uptake rate. That variation in cell uptake among the three WBC subtypes was in line with what was previously described using solely fluorescently labeled pristine PS-NPLs ranging from 50 to 900 nm (Ballesteros et al., 2020). Moreover, the internalization pattern was different depending on the studied NPL. Taking pristine PS-NPLs as a reference, we observed that NPL surface modifications were relevant for the cellular uptake capacity, modulating the NPL internalization ability. PS-COOH-NPLs showed the highest uptake capacity being significantly different from pristine PS-NPLs in the three cell populations. On the other hand, PS-NH_2-NPLs internalized much less, approximately half compared to PS-COOH- and were not significantly relevant when compared to pristine PS-NPLs. These differences in internalization result for surface modifications and the consequent changes in z-potential values (Martín-Pérez et al., 2024). When the NPL used in the exposure were *true-to-life* (PET or PLA), and compared with commercial pristine PS, the internalization ratio was also different. PLA-NPLs showed a higher uptake capacity in the three WBC populations, being significantly different for PMNs and monocytes. On the other hand, PET-NPL uptake was only relevant and significantly different from pristine PS-NPLs in monocytes. When the results of the donors we separated according to their sex, no significant differences were observed.

The cellular uptake of particles typically initiates with an interaction with the cell membrane, followed by particle entry into cells through passive penetration or active endocytosis processes, which include pinocytosis and phagocytosis (Sousa de Almeida et al., 2021). Phagocytosis predominantly occurs in specialized cells like macrophages, monocytes, eosinophils, neutrophils, and dendritic cells, facilitating the engulfment and elimination of foreign bodies and cell debris (Liu et al., 2021). Monocytes and PMNs exhibit a higher rate of nanoparticle internalization, attributed to their phagocytic behavior, compared to lymphocytes. Despite phagocytosis being traditionally linked to larger particles, studies indicate its occurrence with nanoscale particles, possibly after an opsonization process (Moreno-Mendieta et al., 2022). In contrast to MPLs, NPLs can be internalized through various mechanisms, including pinocytosis, phagocytosis, and receptor-mediated endocytosis (Schröter and Ventura, 2022), potentially explaining their uptake in lymphocytes, albeit limited. During exposure, circulating NPLs interact not only with blood cells but also with biomolecules suspended in blood, leading to the formation of a bio-corona on their surfaces. The bio-corona composition is influenced by blood biomolecules and NPL surface characteristics, such as hydrophobicity and surface charges, which determine NPL behavior (Singh et al., 2021). Plastic polymers and surface modifications of NPLs can affect bio-corona presence, impacting

cellular adhesion and internalization (Gopinath et al., 2021). Phagocytic cells demonstrate varying efficiency in internalizing particles of different sizes and shapes. While rod-shaped particles exhibit reduced phagocytosis, neutrophil association significantly increases with them (Safari et al., 2020). In our study, spherical NPLs with diverse molecular weight distributions were tested, leading to polydispersity in surface potential and size, potentially affecting aggregation and behavior across various cell populations.

3.4. Oxidative stress induction in WBC exposed to NPLs

To investigate the effect of NPLs exposure on oxidative stress status, the intercellular reactive oxygen species (iROS) levels in the different WBC cell subtypes were investigated. As a novelty, and according to the different internalization rates, the analysis was specifically conducted on cells that had internalized NPLs. This approach avoids masking effects that might be observed when considering the entire population (cells with NPLs plus cells without NPLs). This could occur in the lymphocyte population, where the percentage of internalization was very small. This approach has been already demonstrated by Collin-Faure and colleagues, where the higher the internalization of PS-NPLs within a population of macrophages the more pronounced and significant the effects (Collin-Faure et al., 2023).

Our results showed that pristine PS-, PET-, and PLA-NPLs exposure significantly induced intracellular ROS in those WBC with internalized NPLs. The obtained average fold changes were 6.41 (PS-), 6.12 (PET-), and 2.35 (PLA-). Nevertheless, when the iROS analysis is performed in the three WBC populations separately (PMNs, lymphocytes, and monocytes) the highest percentage of iROS observed in the overall cell analysis is attributed to lymphocytes (Fig. 4). This phenomenon is mainly observed in blood samples exposed to PS- and PLA-NPLs; however, in the case of PET-NPLs, all three WBC populations exhibited a significant production of iROS.

The involvement of ROS in the systemic toxicity of MNPLs has been recently reviewed (Das, 2023). Although several studies have demonstrated that MNPLs can target mitochondria, leading to the generation of different types of reactive free radicals, there is a lack of proper models to extrapolate these effects to human health. In this context, the use of *ex vivo* approaches using whole human blood stands out. Effects of MNPLs on human blood include plasma protein denaturation, hemolysis, reduced immunity, thrombosis, blood coagulation, and vascular endothelial damage, among others, which can lead to life-threatening diseases (Rajendran and Chandrasekaran, 2023). All this highlights the relevance of using human blood samples as a target model to determine the effects of MNPL. This model was also successfully used to demonstrate that different types of graphene-based nanomaterials with biomedical applications alter the human blood secretome (Ballesteros et al., 2021). Moreover, the growing interest in bioplastic for drug delivery (Mythri and Aishwarya, 2023) could increase the presence of MNPLs contacting blood components and induce a wide range of effects, including increased ROS levels. Under physiological conditions, ROS are fundamental in cellular signal transduction responding to stress (Fichman et al., 2023), and an excess of ROS is normally produced by WBCs as a host defense response promoting the clearance of pathogens and foreign particles. However, if ROS generation is chronically maintained, the cellular antioxidant system will be overwhelmed and oxidative stress, cell injury, and potentially cell death will be induced (Pizzino et al., 2017). Further investigations might be useful to decipher the potential risk of chronic exposures to MNPLs.

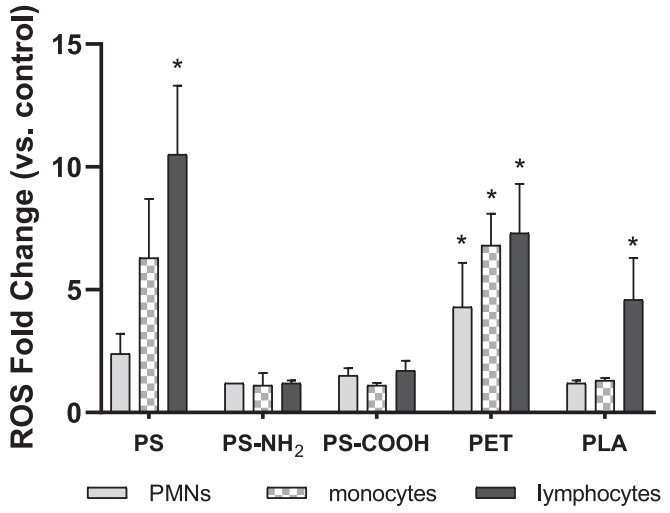

Fig. 4. Relative ROS production in the different white blood cell populations that had internalized NPLs (relative to the unexposed samples), treated with 100 μg/mL of NPLs for 24 h detected by the DHE assay. Data are represented as mean ± SEM and analyzed by the one-way ANOVA. * ($p \leq 0.05$) in front of unexposed cell samples. PMN: polymorphonucleated cells.

Taken together, our results point out two important aspects. First, only cells that have internalized NPLs should be considered in the analysis, to avoid masking positive results in case the internalization rate is not 100 %. Second, when working with heterogeneous cell populations (as in the case of WBC) the endpoint analysis should be performed considering each population separately to avoid deviations due to the different behavior of each cell subtype.

3.5. Immune response

To determine the potential effect of NPLs on the immune response, the blood cytokine secretome after NPLs exposure was analyzed. Thus, a wide battery of 102 cytokines was analyzed in the plasma from exposed

Table 2
Cytokine enhanced release in plasma after NPLs 24 h-exposure. Mean relative cytokine secretion for each NPL is shown as fold change relative to the unexposed whole blood controls. Green color scale indicating the fold change in plasma cytokine levels based on the NPL to which the blood has been exposed. The darker the color, the greater the change relative to the control not exposed to NPLs.

	PS	PS-NH_2	PS-COOH	PLA	PET
CXCL5	2.09	4.03	2.08	8.38	2.94
CCL2	1.46	2.28	2.03	2.81	2.54
CCL7	1.75	6.64	2.65	10.75	1.41
CXCL8	1.29	3.06	1.87	3.10	2.36
CXCL10	1.09	13.03	1.31	2.63	2.72
Leptin	2.04	1.87	2.23	0.59	0.73
CXCL-1	1.35	3.31	1.33	4.83	1.67
CCL20	1.58	20.51	1.64	16.52	1.86
CCL3/CCL4	1.04	18.08	1.65	18.19	1.57
CXCL9	1.05	7.39	1.30	1.37	1.46
IL-24	1.00	2.58	1.32	1.83	1.40
IL-1b	0.83	2.61	1.26	1.14	1.16
IL-6	0.98	4.94	1.32	1.34	1.03
TNF-α	0.85	2.18	1.48	1.74	0.95
PTX3	1.10	1.65	1.24	2.20	1.44
Dkk-1	1.29	1.32	1.48	2.09	1.18
CSF1	0.89	1.38	1.69	11.27	1.38
GDF-15	1.15	1.17	1.43	2.07	1.07
BDNF	1.24	0.91	1.25	2.20	1.74
HGF	1.13	1.79	1.40	2.31	1.88
IL-16	1.12	1.40	1.20	2.29	1.46
VEGF	1.47	1.20	1.10	2.18	0.88
FLT3LG	1.20	1.32	1.52	2.06	1.27
IL-3	1.19	1.66	1.07	1.61	2.20

blood and compared to control (unexposed) blood. Our results show how only 24 h of exposure to the different NPLs highly affected the release of cytokines. Importantly, all the differently expressed cytokines had an enhanced expression, compared to the control sample, and were described as pro-inflammatory cytokines, mostly associated with chemotaxis functions (Hughes and Nibbs, 2018). The effect levels varied between the tested NPLs, being more notably altered after PS-NH_2- and PLA-NPL exposures, and with the mildest affectation due to PS-NPLs. Table 2 shows only those cytokines showing fold changes $\geq$2 for any of the evaluated NPLs. Supplementary Table S2 shows all the data corresponding to the overall panel. Interestingly, PS-NH_2 also induced more harmful effects in human primary endothelial cells than pristine and PS-COOH forms (Martín-Pérez et al., 2024).

As remarkable, all the NPLs induced the overexpression of the chemokine CXCL5. Elevated levels of CXCL5 are detected in blood in several inflammatory and fibrotic diseases including atherosclerosis, pancreatitis, inflammatory bowel disease, sarcoidosis, idiopathic pulmonary fibrosis, endometriosis, rheumatoid arthritis, and other inflammatory autoimmune diseases. CXCL5 has also been associated with several types of cancers (as gastric, colorectal, pancreatic, head and neck squamous cell, and non-small cell lung cancer), whereby it has been related to tumor cell proliferation, angiogenesis, epithelial-mesenchymal transition, and metastatic cell migration (Gencer et al., 2021). Thus, the release of this chemokine, as a response to NPL exposure, might implicate a relevant neutrophil chemoattraction and pro-angiogenic stimulus, that interplay in the regulation of innate immunity, causing possible deregulation in the normal ways of immune activation. The observed cytokine induction panel was different depending on the type of NPLs tested, being mostly affected after PS-NH_2- and PLA-NPL exposure. PS-NH_2-NPLs activated the release of chemokines mainly secreted by monocytes and associated with WBC chemotaxis (such as CXCL5, CCL2, CCL7, CXCL8, CXCL10, CXCL1, CCL20, CCL3/CCL4, and CXCL9). On the other hand, PLA-NPLs not only enhanced chemokines such as PS-NH_2-NPLs, but also other cytokines with functions in the regulation of survival, proliferation, and differentiation of WBCs (*e.g.*, Dkk-1, CSF1, GDF-15, BDNF, HGF, VEGF, and FLT3LG).

To our knowledge, this is the first study investigating the effects on cytokine release of different NPLs in whole blood as a model. Although the idea that exposure to MNPLs induces inflammation has been previously reviewed (Danopoulos et al., 2022; Yang et al., 2022), few authors have studied MNPLs' effects on cytokine secretion and only in individual non-immune cell types. A study showed up-regulated mRNA expression of *IL-1b*, *IL-6*, *IL-8*, and *TNFα* genes in A549 lung cells exposed to PS-NPL alone, or combined with phthalate esters (Shi et al., 2021). Also, the secretion of a panel of inflammatory cytokines was triggered after PS-MNPLs exposure to the human intestinal organoid-derived epithelial tissue model (Chen et al., 2023). Although different authors have shown how MNPLs stimulate the release of pro-inflammatory cytokines using different approaches (Panizzolo et al., 2023), most of these studies have been carried out using PS-MNPLs only, and no information is available about the response triggered by exposure to *true-to-life* materials that better reflect the environmental situation. In addition, very little research has been performed on the effects of NPLs on human blood as an *ex vivo* model in which primary human cells can express their potentiality (Ballesteros et al., 2020). Altogether, our results might help to predict the modulatory effects of the immune system mediated by *true-to-life* NPLs and potential inflammation-mediated toxicity which could affect human health, especially under chronic exposure scenarios.

3.6. Hemolysis induced by NPLs

The sensitivity of erythrocytes to the presence of NPLs was determined by calculating their hemolytic effects. As shown in Fig. 5, both PS- and PS-COOH-NPLs exhibited high levels of hemolysis. In contrast, low levels of hemolysis were found when erythrocyte suspensions were exposed to PS-NH_2-NPLs (4 % lysis) or PET-NPLs (3 % lysis). No

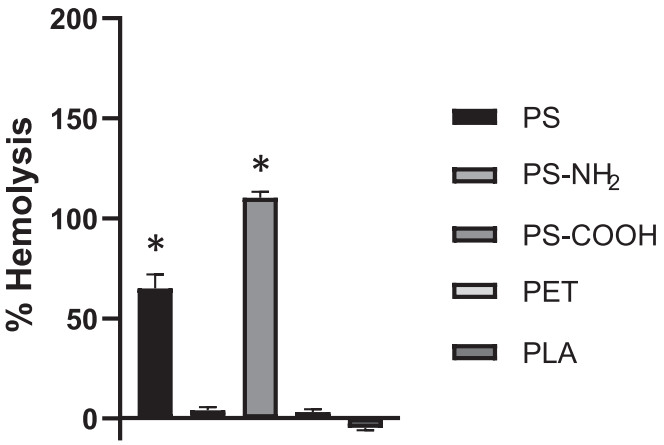

Fig. 5. Hemolytic activity of the different NPLs. The percentage of hemolysis was calculated by subtracting the measured absorbance of the negative sample from the exposed samples with NPLs Then, samples were normalized to the OD of Triton X-100-treated erythrocyte samples and multiplied by 100. Data are represented as mean ± SEM and analyzed by the one-way ANOVA. $^*p \leq 0.05$.

hemolytic signals were observed after PLA-NPL exposure. Previous studies reported hemolytic activity depending on the size of the PS-NPLs (Hwang et al., 2020) and the surface modifications present in NPLs (Kim et al., 2022), but both studies were carried out in isolated erythrocytes. However, no previous data is available related to PLA or PET NPLs effects.

Although some studies exist, mainly based on the hemolytic effect of nanomaterials used in medicine (Yedgar et al., 2022), the mechanism by which NPLs can induce hemolysis has not yet been defined. The level of cell hemolysis might be dependent on the interaction between the NPLs and the erythrocytes; thus, the contact of NPLs with the cells may destabilize the membrane and cause defects leading to cell hemolysis. In *in vivo* studies, the hemolytic effects observed in mice exposed to PS-MPLs were associated with changes in the typical erythrocyte structure, resulting in numerous aberrant shapes (Abdel-Zaher et al., 2023). Accordingly, the size of the MNPLs and their surface functionalization would determine the nature of their interaction with the cell membrane and their potentially harmful effects, as described in the previous sections.

3.7. Coagulation and platelet functionality

Erythrocyte membrane breaks could accelerate coagulation reactions (Kim et al., 2022), and it is known that plasma protein interactions with artificial surfaces could trigger the coagulation process, resulting in thrombus production and the formation of a fibrin clot (Xu et al., 2014). In this context, the effects of NPLs on the coagulation process were evaluated by determining the major clinically used clotting tests, including prothrombin time (INR, International Normalized Ratio) (PT), activated partial thromboplastin time (aPTT), prothrombin time (in seconds) (TT), and fibrin concentration (FIB). Although no significant differences between NPLs exposed and control blood samples were observed in any of the performed tests, aPPT values in the PS-COOH-NPLs exposed blood were elevated above the normal range, related to the other samples, but without reaching statistical significance (Table 3). This parameter is related to contact surface-initiation of coagulation (traditionally called intrinsic coagulation pathway) by the activation of FXIIa. Different negatively charged artificial material surfaces can stimulate FXIIa autoactivation, as several pathogenic and physiological agents can do (Simak and De Paoli, 2017). Thus, the negative charges provided by COOH-surface modifications seem to be able to initiate the contact pathway of coagulation, leading to a thrombotic state.

Table 3
Effects of NPLs on coagulation. Data represented as mean ± SEM. PT: prothrombin time (INR: International Normalized Ratio); aPTT: activated partial thromboplastin time; TT: prothrombin time (in seconds); FIB: fibrin concentration.

	Control	PS	PS-NH_2	PS-COOH	PET	Normal range
PT (INR)	1.35 ± 0.05	1.32 ± 0.04	1.31 ± 0.06	1.46 ± 0.08	1.34 ± 0.03	(0.90–1.20)
aPPT (s)	34.4 ± 0.6	35.2 ± 0.8	34.7 ± 1.5	39.7 ± 2.1	36.0 ± 0.3	(24.0–35.0)
TT (s)	16.95 ± 0.25	17.10 ± 0.50	16.90 ± 0.10	17.40 ± 0.10	16.70 ± 0.20	< 21.0
FIB (mg/dL)	300.5 ± 11.5	308.0 ± 14.0	304.5 ± 10.5	305.5 ± 8.5	312.5 ± 8.5	(200–400)

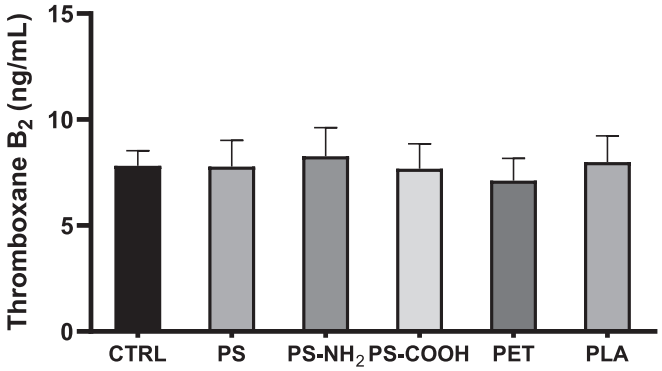

Fig. 6. Presence of thromboxane B_2 in plasma after exposing whole blood samples to 100 μg/mL of NPLs for 24 h. Data are represented as mean ± SEM. CTRL: unexposed control sample.

Because of the important role of platelets in primary hemostasis, the effect of NPLs on human platelet activation was also analyzed by the quantification of the thromboxane B_2 (TXB_2) present in plasma. Upon activation, platelets release markers and antigens such as thromboxane A_2 (TXA_2); however, TXA_2 has an extremely short half-life (around 35 s), and the production of TXA_2 can be monitored by the presence of TXB_2 which is produced by the non-enzymatic hydration of TXA_2, and it is stable (Patrono and Rocca, 2019). Our results showed that NPLs had no significant effect on TXB_2 production. Thus, platelets were not activated after NPLs exposure in whole blood (Fig. 6).

Although no studies have been found linking MNPL exposure and thromboxane B_2 release, its released by platelets, as a marker of platelet activation, was evaluated by exposing platelets to silver nanoparticles (AgNPs) with and without poly-ethyl glycol (PEG) functionalization (Hajtuch et al., 2019). The observed results indicated that under all the conditions evaluated, AgNPs significantly reduced the released levels of thromboxane B_2. The potential effects of MNPLs on platelets and thrombosis induction have been determined using human blood exposed to PS-MPLs observing thrombus formation effects in mass and structure (Chen et al., 2022). Interestingly, using an on-chip model confirmed such effects, PS-MPL exposure leading to decreased binding strength of fibrin to platelets. *In vivo* studies conducted with zebrafish showed the PS-MPLs exposure activated platelets to aggregate in damaged regions enhancing the coagulation function of platelets, and facilitating fibrin clots formation (Gao et al., 2021). This role of MNPLs in thrombus formation has been demonstrated in human thrombi where microplastics were detected using Raman spectrometry (Wu et al., 2023b). These findings would confirm the results showing that surface modifications of PS-MNPLs can affect *in vitro* whole blood clotting dynamics. Thus, by comparing carboxylated, aminated, and non-functionalized PS-MNPLs authors showed that, by using thrombo-elastography, carboxylated forms consistently activated the clotting cascade, increasing fibrin polymerization rates, and enhancing clot strength. Aminated forms exert similar but reduced effects, and those induced by the non-functionalized form showed minimal effects (Christodoulides et al., 2023). All the above-reported studies would indicate that the prolonged presence of MNPLs in blood could affect bloodstream functionality. As previously commented, surface modifications can affect z-potential values, modulating PDI parameters and cell internalization, both as total internalized particles and time-related uptake. As a resulting outcome, the evaluated hazardous effects are modulated by surface functionalizations (Martín-Pérez et al., 2024).

4. Conclusions

This article provides the first report on the toxic effects of various types of NPLs on the human bloodstream. Once NPLs cross the biological barriers (gut and lung epithelium) the first target is blood. Therefore, it is of relevance to elucidate the potential interactions between blood components and NPLs, to understand the health risks posed by environmental NPLs.

Utilizing an *ex vivo* model such as the extraction of peripheral human blood from healthy donors, we have been able to show the different rates of internalization of three different surface-functionalized PS (commercially available), and two *true-to-life* NPLs (PLA and PET) in the three major WBC subtypes: lymphocytes, PMNs, and monocytes.

Through this study, focusing on the different types of commercial PS-NPLs, we observed that PS-NPL surface modifications were relevant for their cellular uptake capacity. Carboxylated surfaces enhanced the NPLs' ability to internalize in the three WBC subtypes studied when compared to pristine PS-NPLs, which only internalized in monocytes, or to aminated PS-NPLs that are capable of internalizing at a higher rate than pristine PS, but only in PMNs and monocytes. When *true-to-life* (PET or PLA) NPLs were used, the observed internalization ratio was different. PLA-NPLs showed a higher uptake capacity in the three WBC populations, being significantly different for PMNs and monocytes. On the other hand, PET-NPL uptake was only relevant and significantly different from pristine PS-NPLs in monocytes. When the results of the different donors were separated, based on their sex, no significant differences were obtained.

Regarding the induced effects, pristine PS-NPLs significantly increased the production of iROS in lymphocytes, as well as generating high levels of hemolysis; on the contrary, PS-NH_2-NPLs do not provoke the generation of iROS nor cause hemolysis but induced the secretion of many proinflammatory cytokines, especially those related to WBC chemotaxis. PS-COOH-NPLs did not induce the generation of iROS and the secretion of proinflammatory cytokines was modest; nonetheless, its exposure resulted in significant hemolysis induction. PET-NPLs generated significant levels of iROS in all three cellular subtypes of WBCs. while PLA-NPLs cause a significant generation of iROS in lymphocytes, inducing the secretion of many proinflammatory cytokines related to leukocyte chemotaxis and their proliferation, survival, and differentiation. Fig. 7 shows a quick overview of all the obtained results.

A particular point of interest in our study is the use of only NPLs-containing cells to determine potential effects. This avoids false-negative results derived from measuring the response in a mix of subpopulations with a variable proportion of cells that internalized NPLs. The use of an array of cytokines, instead of using a cytokine-candidate approach, is another aspect to point out. Thus, using a panel of 102 cytokines avoids any type of experimental bias. Interestingly, differences were observed after exposures, with higher effects after PLA- and PS-NH_2-NPL exposure. A total of 24 cytokines were overexpressed with a fold ≥2, CCL20 and CCL3/4 being the most highly expressed and CXCL5 the only expressed under all exposed NPLs.

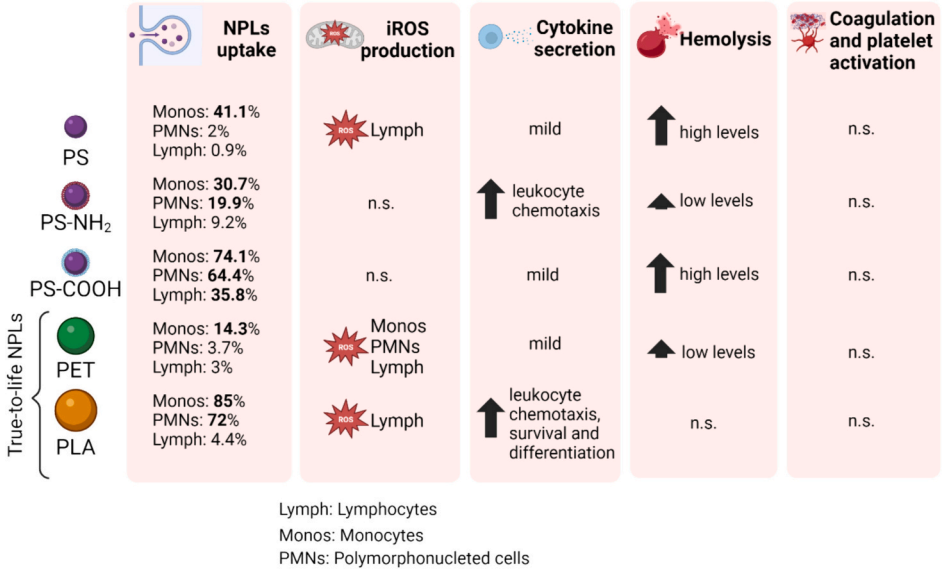

Fig. 7. Summing up the relevant results obtained in the present study.

On the other side, blood-related functional assays including hemolysis, coagulation, and platelet functionality were also included, which is not a generalized topic included in this type of study. Accordingly, we have demonstrated hemolysis induction after PS- and PS-NCOOH-NPL exposure. Finally, although no significant effects on coagulation and platelet functionality were observed, we hypothesize that the negative charges provided by COOH surface modifications could initiate the contact pathway of coagulation, leading to a thrombotic state.

Regarding the study's weakness, we are aware that only one concentration (100 μg/mL) and one exposure time (24 h) were assayed. Nevertheless, the complexity of the experimental design limited the exposure conditions to assess the effects of multiple types of polymeric nanoplastics. However, the obtained results are extremely relevant, since our methodological/technical efforts and novel approaches have helped to reveal the distinct ability of NPLs to interact in a complex tissue matrix as is whole blood, where in addition to the different cell subtypes, a complex mixture of proteins and other biomolecules exist.

CRediT authorship contribution statement

J. Arribas Arranz: Writing – original draft, Methodology, Formal analysis. **A. Villacorta:** Methodology, Investigation. **L. Rubio:** Validation, Methodology, Investigation. **A. García-Rodríguez:** Validation, Methodology, Investigation. **G. Sánchez:** Supervision. **M. Llorca:** Supervision. **M. Farre:** Supervision. **J.F. Ferrer:** Methodology, Investigation. **R. Marcos:** Writing – review & editing, Supervision, Conceptualization. **A. Hernández:** Writing – review & editing, Funding acquisition, Conceptualization.

Declaration of competing interest

The authors declare that they have no known competing financial interests or personal relationships that could have appeared to influence the work reported in this paper.

Data availability

Data will be made available on request.

Acknowledgments

A. Villacorta was supported by Ph.D. fellowships from the National Agency for Research and Development (ANID), CONICYT PFCHA/DOCTORADO BECAS CHILE/2020-72210237. A. García-Rodríguez received funding from the postdoctoral fellowship program Beatriu de Pinós, funded by the Secretary of Universities and Research [Government of Catalonia] and by the Horizon 2020 program of Research and Innovation of the European Union under the Marie Sktodowsdka-Curie grant agreement No 801370. L. Rubio holds a postdoctoral Juan de la Cierva contract (IJC2020–2686I/AEI/10.13039/501100011033). A. Hernández was granted an ICREA ACADEMIA award.

This project (PlasticHeal) has received funding from the European Union's Horizon 2020 research and innovation programme under grant agreement No 965196. This work was partially supported by the Spanish Ministry of Science and Innovation [PID2020-116789, RB-C43] and the Generalitat de Catalunya (2021-SGR-00731).

Appendix A. Supplementary data

Supplementary data to this article can be found online at https://doi.org/10.1016/j.scitotenv.2024.174725.

References

Abdel-Zaher, S., Mohamed, M.S., Sayed, A.E.H., 2023. Hemotoxic effects of polyethylene microplastics on mice. Front. Physiol. 14, 1072797 https://doi.org/10.3389/fphys.2023.1072797.

Alaraby, M., Abass, D., Hernández, A., Marcos, R., 2024. Are bioplastics safe? Hazardous effects of polylactic acid (PLA) nanoplastics in *Drosophila*. Sci. Total Environ. 919, 170592 https://doi.org/10.1016/j.scitotenv.2024.170592.

Altan-Bonnet, G., Mukherjee, R., 2019. Cytokine-mediated communication: a quantitative appraisal of immune complexity. Nat. Rev. Immunol. 19, 205–217. https://doi.org/10.1038/s41577-019-0131-x.

Auguste, M., Balbi, T., Ciacci, C., Canonico, B., Papa, S., Borello, A., Vezzulli, L., Canesi, L., 2020. Shift in immune parameters after repeated exposure to nanoplastics in the marine bivalve *Mytilus*. Front. Immunol. 11, 426. https://doi.org/10.3389/fimmu.2020.00426.

Ballesteros, S., Domenech, J., Barguilla, I., Cortés, C., Marcos, R., Hernández, A., 2020. Genotoxic and immunomodulatory effects in human white blood cells after *ex vivo* exposure to polystyrene nanoplastics. Environ. Sci. Nano 7 (11), 3431–3446. https://doi.org/10.1039/D0EN00748J.

Ballesteros, S., Domenech, J., Velázquez, A., Marcos, R., Hernández, A., 2021. *Ex vivo* exposure to different types of graphene-based nanomaterials consistently alters human blood secretome. J. Hazard. Mater. 414, 125471 https://doi.org/10.1016/j.jhazmat.2021.125471.

Banaei, G., García-Rodríguez, A., Tavakolpournegari, A., Martín-Pérez, J., Villacorta, A., Marcos, R., Hernández, A., 2023. The release of polylactic acid nanoplastics (PLA-NPLs) from commercial teabags. Obtention, characterization, and hazard effects of true-to-life PLA-NPLs. J. Hazard. Mater. 458, 131899 https://doi.org/10.1016/j.jhazmat.2023.131899.

Brandts, I., Teles, M., Gonçalves, A.P., Barreto, A., Franco-Martinez, L., Tvarijonaviciute, A., Martins, M.A., Soares, A.M.V.M., Tort, L., Oliveira, M., 2018. Effects of nanoplastics on *Mytilus galloprovincialis* after individual and combined exposure with carbamazepine. Sci. Total Environ. 643, 775–784. https://doi.org/10.1016/j.scitotenv.2018.06.257.

Byrnes, J.R., Wolberg, A.S., 2017. Red blood cells in thrombosis. Blood 130 (16), 1795–1799. https://doi.org/10.1182/blood-2017-03-745349.

Chen, L., Zheng, Y., Liu, Y., Tian, P., Yu, L., Bai, L., Zhou, F., Yang, Y., Cheng, Y., Wang, F., Zheng, L., Jiang, F., Zhu, Y., 2022. Microfluidic-based *in vitro* thrombosis model for studying microplastics toxicity. Lab Chip 22 (7), 1344–1353. https://doi.org/10.1039/d1lc00989c.

Chen, Y., Williams, A.M., Gordon, E.B., Rudolph, S.E., Longo, B.N., Li, G., Kaplan, D.L., 2023. Biological effects of polystyrene micro- and nano-plastics on human intestinal organoid-derived epithelial tissue models without and with M cells. Nanomed.: Nanotechnol., Biol. Med. 50, 102680 https://doi.org/10.1016/j.nano.2023.102680.

Christodoulides, A., Hall, A., Alves, N.J., 2023. Exploring microplastic impact on whole blood clotting dynamics utilizing thromboelastography. Front. Public Health 11, 1215817. https://doi.org/10.3389/fpubh.2023.1215817.

Collin-Faure, V., Vitipon, M., Torres, A., Tanyeres, O., Dalzon, B., Rabilloud, T., 2023. The internal dose makes the poison: higher internalization of polystyrene particles induces increased perturbation of macrophages. Front. Immunol. 14, 1092743 https://doi.org/10.3389/fimmu.2023.1092743.

Danopoulos, E., Twiddy, M., West, R., Rotchell, J.M., 2022. A rapid review and meta-regression analyses of the toxicological impacts of microplastic exposure in human cells. J. Hazard. Mater. 427, 127861 https://doi.org/10.1016/j.jhazmat.2021.127861.

Das, A., 2023. The emerging role of microplastics in systemic toxicity: involvement of reactive oxygen species (ROS). Sci. Total Environ. 895, 165076 https://doi.org/10.1016/j.scitotenv.2023.165076.

Evans, B.C., Nelson, C.E., Yu, S.S., Beavers, K.R., Kim, A.J., Li, H., Nelson, H.M., Giorgio, T.D., Duvall, C.L., 2013. *Ex vivo* red blood cell hemolysis assay for the evaluation of pH-responsive endosomolytic agents for cytosolic delivery of biomacromolecular drugs. J. Vis. Exp. JoVE 73, 50166. https://doi.org/10.3791/50166.

Fichman, Y., Rowland, L., Oliver, M.J., Mittler, R., 2023. ROS are evolutionary conserved cell-to-cell stress signals. Proc. Natl. Acad. Sci. U. S. A. 120 (31), e2305496120 https://doi.org/10.1073/pnas.2305496120.

Gao, N., Huang, Z., Xing, J., Zhang, S., Hou, J., 2021. Impact and molecular mechanism of microplastics on zebrafish in the presence and absence of copper nanoparticles. Front. Mar. Sci. 8, 2021. https://doi.org/10.3389/fmars.2021.762530.

Gencer, S., Evans, B.R., van der Vorst, E.P.C., Döring, Y., Weber, C., 2021. Inflammatory chemokines in atherosclerosis. Cells 10 (2), 226. https://doi.org/10.3390/cells10020226.

Gopinath, P.M., Twayana, K.S., Ravanan, P., Thomas, John, Mukherjee, A., Jenkins, D.F., Chandrasekaran, N., 2021. Prospects on the nano-plastic particles internalization and induction of cellular response in human keratinocytes. Part. Fibre Toxicol. 18 (1), 35. https://doi.org/10.1186/s12989-021-00428-9.

Greven, A.-C., Merk, T., Karagöz, F., Mohr, K., Klapper, M., Jovanović, B., Palić, D., 2016. Polycarbonate and polystyrene nanoplastic particles act as stressors to the innate immune system of fathead minnow (*Pimephales promelas*). Environ. Toxicol. Chem. 35 (12), 3093–3100. https://doi.org/10.1002/etc.3501.

Hajtuch, J., Hante, N., Tomczyk, E., Wojcik, M., Radomski, M.W., Santos-Martinez, M.J., Inkielewicz-Stepniak, I., 2019. Effects of functionalized silver nanoparticles on aggregation of human blood platelets. Int. J. Nanomedicine 14, 7399–7417. https://doi.org/10.2147/IJN.S213499.

Helgadóttir, H., Ólafsson, Í., Andersen, K., Gizurarson, S., 2019. Stability of thromboxane in blood samples. Vasc. Health Risk Manag. 15, 143–147. https://doi.org/10.2147/VHRM.S204925.

Hughes, C.E., Nibbs, R.J.B., 2018. A guide to chemokines and their receptors. FEBS J. 285 (16), 2944–2971. https://doi.org/10.1111/febs.14466.

Hwang, J., Choi, D., Han, S., Jung, S.Y., Choi, J., Hong, J., 2020. Potential toxicity of polystyrene microplastic particles. Sci. Rep. 10 (1), 7391. https://doi.org/10.1038/s41598-020-64464-9.

Kim, E.H., Choi, S., Kim, D., Park, H.J., Bian, Y., Choi, S.H., Chung, H.Y., Bae, O.N., 2022. Amine-modified nanoplastics promote the procoagulant activation of isolated human red blood cells and thrombus formation in rats. Part. Fibre Toxicol. 19, 60. https://doi.org/10.1186/s12989-022-00500-y.

Landrigan, P.J., Raps, H., Cropper, M., Bald, C., Brunner, M., Canonizado, E.M., Charles, D., Chiles, T.C., Donohue, M.J., Enck, J., Fenichel, P., Fleming, L.E., Ferrier-Pages, C., Fordham, R., Gozt, A., Griffin, C., Hahn, M.E., Haryanto, B., Hixson, R., Ianelli, H., James, B.D., Kumar, P., Laborde, A., Law, K.L., Martin, K., Mu, J., Mulders, Y., Mustapha, A., Niu, J., Pahl, S., Park, Y., Pedrotti, M.L., Pitt, J.A., Ruchirawat, M., Seewoo, B.J., Spring, M., Stegeman, J.J., Suk, W., Symeonides, C., Takada, H., Thompson, R.C., Vicini, A., Wang, Z., Whitman, E., Wirth, D., Wolff, M., Yousuf, A.K., Dunlop, S., 2023. The Minderoo-Monaco commission on plastics and human health. Ann. Glob. Health 89 (1), 23. https://doi.org/10.5334/aogh.4056.

Leslie, H.A., van Velzen, M.J.M., Brandsma, S.H., Vethaak, A.D., Garcia-Vallejo, J.J., Lamoree, M.H., 2022. Discovery and quantification of plastic particle pollution in human blood. Environ. Int. 163, 107199 https://doi.org/10.1016/j.envint.2022.107199.

Liu, L., Xu, K., Zhang, B., Ye, Y., Zhang, Q., Jiang, W., 2021. Cellular internalization and release of polystyrene microplastics and nanoplastics. Sci. Total Environ. 779, 146523 https://doi.org/10.1016/j.scitotenv.2021.146523.

Martín-Pérez, J., Villacorta, A., Banaei, G., Morataya-Reyes, M., Tavakolpournegari, A., Marcos, R., Hernández, A., García-Rodríguez, A., 2024. Hazard assessment of nanoplastics is driven by their surface-functionalization. Effects in human-derived primary endothelial cells. Sci. Total Environ. 934, 173236 https://doi.org/10.1016/j.scitotenv.2024.173236.

Matus, M.F., Vilos, C., Cisterna, B.A., Fuentes, E., Palomo, I., 2018. Nanotechnology and primary hemostasis: differential effects of nanoparticles on platelet responses. Vascul. Pharmacol. 101, 1–8. https://doi.org/10.1016/J.VPH.2017.11.004.

Moreno-Mendieta, S., Guillén, D., Vasquez-Martínez, N., Hernández-Pando, R., Sánchez, S., Rodríguez-Sanoja, R., 2022. Understanding the phagocytosis of particles: the key for rational design of vaccines and therapeutics. Pharm. Res. 39 (8), 1823–1849. https://doi.org/10.1007/s11095-022-03301-2.

Mythri, R.B., Aishwarya, M.R.B., 2023. Biopolymers as promising vehicles for drug delivery to the brain. Drug Metab. Rev. 13, 1–16. https://doi.org/10.1080/03602532.2023.2281855.

Panizzolo, M., Martins, V.H., Ghelli, F., Squillacioti, G., Bellisario, V., Garzaro, G., Bosio, D., Colombi, N., Bono, R., Bergamaschi, E., 2023. Biomarkers of oxidative stress, inflammation, and genotoxicity to assess exposure to micro- and nanoplastics. A literature review. Ecotoxicol. Environ. Saf. 267, 115645 https://doi.org/10.1016/j.ecoenv.2023.115645.

Patrono, C., Rocca, B., 2019. Measurement of thromboxane biosynthesis in health and disease. Front. Pharmacol. 10, 1244. https://doi.org/10.3389/FPHAR.2019.01244/BIBTEX.

Pizzino, G., Irrera, N., Cucinotta, M., Pallio, G., Mannino, F., Arcoraci, V., Squadrito, F., Altavilla, D., Bitto, A., 2017. Oxidative stress: harms and benefits for human health. Oxid. Med. Cell. Longev. 2017, 8416763 https://doi.org/10.1155/2017/8416763.

Rajendran, D., Chandrasekaran, N., 2023. Journey of micronanoplastics with blood components. RSC Adv. 13 (45), 31435–31459. https://doi.org/10.1039/d3ra05620a.

Ramsperger, A.F.R.M., Bergamaschi, E., Panizzolo, M., Fenoglio, I., Barbero, F., Peters, R., Undas, A., Purker, S., Giese, B., Lalyer, C.R., Tamargo, A., Moreno-Arribas, M.V., Grossart, H.P., Kühnel, D., Dietrich, J., Paulsen, F., Afanou, A.K., Zienolddiny-Narui, S., Eriksen Hammer, S., Kringlen Ervik, T., Graff, P., Brinchmann, B.C., Nordby, K.C., Wallin, H., Nassi, M., Benetti, F., Zanella, M., Brehm, J., Kress, H., Löder, M.G.J., Laforsch, C., 2023. Nano- and microplastics: a comprehensive review on their exposure routes, translocation, and fate in humans. NanoImpact 29, 100441. https://doi.org/10.1016/j.impact.2022.100441.

Rubio, L., Marcos, R., Hernández, A., 2020. Potential adverse health effects of ingested micro- and nanoplastics on humans. Lessons learned from *in vivo* and *in vitro* mammalian models. J. Toxicol. Environ. Health B Crit. Rev. 23 (2), 51–68. https://doi.org/10.1080/10937404.2019.1700598.

Safari, H., Kelley, W.J., Saito, E., Kaczorowski, N., Carethers, L., Shea, L.D., Eniola-Adefeso, O., 2020. Neutrophils preferentially phagocytose elongated particles -an opportunity for selective targeting in acute inflammatory diseases. Sci. Adv. 6 (24), eaba1474 https://doi.org/10.1126/sciadv.aba1474.

Sarma, D.K., Dubey, R., Samarth, R.M., Shubham, S., Chowdhury, P., Kumawat, M., Verma, V., Tiwari, R.R., Kumar, M., 2022. The biological effects of polystyrene nanoplastics on human peripheral blood lymphocytes. Nanomaterials 12 (10), 1632. https://doi.org/10.3390/nano12101632.

Schröter, L., Ventura, N., 2022. Nanoplastic toxicity: insights and challenges from experimental model systems. Small 18 (31), e2201680. https://doi.org/10.1002/smll.202201680.

Shi, Q., Tang, J., Wang, L., Liu, R., Giesy, J.P., 2021. Combined cytotoxicity of polystyrene nanoplastics and phthalate esters on human lung epithelial A549 cells and its mechanism. Ecotoxicol. Environ. Saf. 213, 112041 https://doi.org/10.1016/j.ecoenv.2021.112041.

Simak, J., De Paoli, S., 2017. The effects of nanomaterials on blood coagulation in hemostasis and thrombosis. Wiley Interdiscip. Rev. Nanomed. Nanobiotechnol. 9 (5), e1448 https://doi.org/10.1002/WNAN.1448.

Sindhwani, S., Syed, A.M., Ngai, J., Kingston, B.R., Maiorino, L., Rothschild, J., MacMillan, P., Zhang, Y., Rajesh, N.U., Hoang, T., Wu, J.L.Y., Wilhelm, S., Zilman, A., Gadde, S., Sulaiman, A., Ouyang, B., Lin, Z., Wang, L., Egeblad, M., Chan, W.C.W., 2020. The entry of nanoparticles into solid tumours. Nat. Mater. 19 (5), 566–575. https://doi.org/10.1038/s41563-019-0566-2.

Singh, N., Marets, C., Boudon, J., Millot, N., Saviot, L., Maurizi, L., 2021. *In vivo* protein corona on nanoparticles: does the control of all material parameters orient the biological behavior? Nanoscale Adv. 3 (5), 1209–1229. https://doi.org/10.1039/D0NA00863J.

Sousa de Almeida, M., Susnik, E., Drasler, B., Taladriz-Blanco, P., Petri-Fink, A., Rothen-Rutishauser, B., 2021. Understanding nanoparticle endocytosis to improve targeting strategies in nanomedicine. Chem. Soc. Rev. 50 (9), 5397–5434. https://doi.org/10.1039/d0cs01127d.

Tian, Y., Tian, Z., Dong, Y., Wang, X., Zhan, L., 2021. Current advances in nanomaterials affecting morphology, structure, and function of erythrocytes. RSC Adv. 11 (12), 6958–6971. https://doi.org/10.1039/d0ra10124a.

Urbán, P., Liptrott, N.J., Bremer, S., 2019. Overview of the blood compatibility of nanomedicines: a trend analysis of *in vitro* and *in vivo* studies. Wiley Interdiscip. Rev. Nanomed. Nanobiotechnol. 11 (3), e1546 https://doi.org/10.1002/wnan.1546.

van der Meijden, P.E.J., Heemskerk, J.W.M., 2019. Platelet biology and functions: new concepts and clinical perspectives. Nat. Rev. Cardiol. 16 (3), 166–179. https://doi.org/10.1038/s41569-018-0110-0.

Villacorta, A., Rubio, L., Alaraby, M., López-Mesas, M., Fuentes-Cebrian, V., Moriones, O. H., Marcos, R., Hernández, A., 2022. A new source of representative secondary PET nanoplastics, obtention, characterization, and hazard evaluation. J. Hazard. Mater. 439, 129593 https://doi.org/10.1016/J.JHAZMAT.2022.129593.

Villacorta, A., Cazorla-Ares, C., Fuentes-Cebrian, V., Valido, I.H., Vela, L., Carrillo-Navarrete, F., Morataya-Reyes, M., Mejia-Carmona, K., Pastor, S., Velázquez, A., Arribas Arranz, J., Marcos, R., López-Mesas, M., Hernández, A., 2024. Fluorescent labeling of nanoplastics for biological applications with a focus on true-to-life MNPLs

tracking. J. Hazard. Mater. 135134 https://doi.org/10.1016/j.jhazmat.2024.135134.

Wu, D., Feng, Y., Wang, R., Jiang, J., Guan, Q., Yang, X., Wei, H., Xia, Y., Luo, Y., 2023b. Pigment microparticles and microplastics found in human thrombi based on Raman spectral evidence. J. Adv. Res. 49, 141–150. https://doi.org/10.1016/j.jare.2022.09.004.

Wu, Y., Yao, Y., Bai, H., Shimizu, K., Li, R., Zhang, C., 2023a. Investigation of pulmonary toxicity evaluation on mice exposed to polystyrene nanoplastics: the potential protective role of the antioxidant N-acetylcysteine. Sci. Total Environ. 855, 158851 https://doi.org/10.1016/j.scitotenv.2022.158851.

Xu, L.C., Bauer, J., Siedlecki, C.A., 2014. Proteins, platelets, and blood coagulation at biomaterial interfaces. Colloids Surf. B Biointerfaces 124, 49–68. https://doi.org/10.1016/j.colsurfb.2014.09.040.

Yang, W., Jannatun, N., Zeng, Y., Liu, T., Zhang, G., Chen, C., Li, Y., 2022. Impacts of microplastics on immunity. Front. Toxicol. 4, 956885 https://doi.org/10.3389/ftox.2022.956885.

Yedgar, S., Barshtein, G., Gural, A., 2022. Hemolytic activity of nanoparticles as a marker of their hemocompatibility. Micromachines 13 (12), 2091. https://doi.org/10.3390/mi13122091.

Zhou, Y., He, G., Jiang, H., Pan, K., Liu, W., 2023. Nanoplastics induce oxidative stress and triggers lysosome-associated immune-defensive cell death in the earthworm *Eisenia fetida*. Environ. Int. 174, 107899 https://doi.org/10.1016/j.envint.2023.107899.